

# Permanent magnet generator performance comparison under different topologies and capacities

Ketut Wirtayasa, Muhammad Kasim, Puji Widiyanto, Anwar Muqorobin,  
Sulistyo Wijanarko, Pudji Irasari

Research Centre for Energy Conversion and Conservation, National Research and Innovation Agency (BRIN), Serpong, Indonesia

## Article Info

### Article history:

Received Nov 6, 2024

Revised May 9, 2025

Accepted May 25, 2025

### Keywords:

Ansys Maxwell

Axial flux permanent magnet generator

Electrical performance

Mechanical performance

Radial flux permanent magnet generator

## ABSTRACT

This paper compares the magnetic, electrical, and mechanical characteristics of two permanent magnet generator topologies: single-gap axial flux and single-gap inner rotor radial flux. The study aims to identify how the key parameters fluctuate at each power capacity and investigate the trends in their values as power changes. The power capacities observed are 300 W, 600 W, 900 W, 1200 W, and 1500 W. Simulations used with the help of Ansys Maxwell software to obtain: i) magnetic characteristics without load, including air gap flux density, flux linkage, and induced voltage, ii) electrical performance, consisting of armature current, terminal voltage, voltage regulation, total harmonic distortion, core loss and output power, and iii) mechanical performance, including shaft torque and cogging torque. The last step compares the power density of both topologies. The simulation results show that the axial flux permanent magnet generator (AFPMG) has better air gap flux density, voltage regulation, total harmonic distortion (THD), efficiency, electromagnetic torque, and power density characteristics. Meanwhile, the radial flux permanent magnet generator (RFPMG) is superior in induced voltage and output power. These results conclude that, in general, AFPMG is exceptional from a technical point of view and is more economical when applied to hydro or wind energy systems.

*This is an open access article under the [CC BY-SA](#) license.*



## Corresponding Author:

Muhammad Kasim

Research Centre for Energy Conversion and Conservation, National Research and Innovation Agency (BRIN)

Puspiptek Bld 620, Serpong 15314, Indonesia

Email: muha087@brin.go.id

## 1. INTRODUCTION

The growing energy demand necessitates optimizing available resources, especially renewable energy. Significant advancements have focused on optimizing hybrid energy systems, such as solar, diesel, and battery storage, to support standalone energy solutions. For example, research in [1] developed a standalone photovoltaic/diesel/battery system for remote mining sites, while [2] applied the Gray Wolf Algorithm to enhance automatic generation control in deregulated power systems. Additionally, [3] highlighted the importance of selecting efficient algorithms for hybrid PV-diesel systems.

Beyond hybrid systems, there's extensive research into improving renewable energy sources like wind, hydropower, and also for electric vehicle applications. For wind power, studies have optimized permanent magnet generators for small turbines [4], [5], reduced cogging torque [6], and compared generator designs [7], [8]. Hydropower research includes optimized generators for Pico plants [9], [10] and compact plant analysis [11], [12]. In electric vehicles, studies addressed torque ripple in integrated starter and generator machines [13], improved permanent magnet (PM) shapes for axial flux machines [14], and mechanical field weakening for enhanced EV performance [15].

The study compares different aspects of permanent magnet generators (PMGs) from various sources. Previous study [16], rare earth magnets outperform non-rare magnets due to higher magnetic flux density, although non-rare magnets are considered more economically viable. Rare earth magnets also show lower cogging torque and better efficiency [17], and arc-shaped magnets provide higher electromotive force (EMF) and output power than rectangular ones [18]. Comparisons between axial flux permanent magnet generators (AFPMG) and radial flux permanent magnet generators (RFPMG) show AFPMG is better for space-limited applications, while RFPMG offers better cooling and structural robustness [19]. AFPMG generally has superior cooling at higher aspect ratios, but RFPMG can perform well under certain conditions [20]. Studies like [21] found AFPMG outperformed RFPMG in a 550 W comparison, while [22] showed RFPMG had a higher terminal voltage but was heavier. AFPMG showed a higher cost/torque ratio for wind turbine applications [23] and outperformed RFPMG in a 3 kW generator test [24]. Despite higher material costs, AFPMG had lower manufacturing expenses in [25], though [26] found RFPMG outperformed AFPMG in a 300 W test.

While AFPMG often excels, RFPMG can perform better in some cases. Existing studies focus on specific power capacities, leaving a gap in comparing performance across different capacities. This study fills that gap by analyzing AFPMG and RFPMG at power levels from 300 W to 1500 W. It examines parameters like total harmonic distortion (THD), voltage regulation (VR), cogging torque, and others, using finite element analysis (Ansys Maxwell) to assess no-load and on-load magnetic flux, electrical, and mechanical performance, and compares power density for each topology.

The key novelties and main contributions of this study include: i) multi-capacity comparative analysis: Evaluates performance trends at five different power levels to assess scalability effects, whereas previous studies focused on a single power level; ii) Informed generator selection: Examining multiple power capacities provides a structured basis for choosing between AFPMG and RFPMG, ensuring alignment with specific application needs; iii) Comprehensive performance evaluation: Unlike previous studies that analyzed parameters individually or in limited combinations, this work adopts a holistic approach, offering deeper insights into AFPMG-RFPMG trade-offs for researchers and practitioners.

The remaining sections of this work are organized as follows: i) Section 2 explains the study's methodology, which included generator modeling, simulation setup, and parameters analyzed; ii) Section 3 provides and examines the simulation results, which include winding parameters, no-load and on-load characteristics comparison; and iii) Section 4 wraps up the study by summarizing the main findings and identifying potential future research topics.

## 2. METHOD

### 2.1. Method of the study

This work requires several stages to achieve the aims. The first stage is to determine the observed generator capacities, namely 300 W, 600 W, 900 W, 1200 W, and 1500 W, all operating at a maximum speed of 835 rpm. The second stage defines constant parameters and completes a preliminary design for the AFPMG type based on the design procedure described in [7]. The results of the second stage include the main dimensions of the stator and rotor, and the number and diameter of the stator winding required for step three. In the third stage, performing Ansys Maxwell simulations includes magnetostatic and dynamic. Furthermore, the fourth stage constructs an RFPMG with a topology equivalent to the AFPMG for each corresponding power capacity. In the final stage, the characteristics of both generators are compared at each power capacity, and the trend of parameter changes with power variations is analyzed.

### 2.2. Generator modelling

The generator modeling visualizes the generator topology based on data obtained from the preliminary design. The stator, rotor, permanent magnet, and winding materials are also defined. The excitation source stems from 8 PM poles glued on the surface of the rotor core. The PM properties are of N35SH grade, with a remanence magnetic flux density of 1.17 T, a coercivity field strength of 876 kA/m, and an axial length of 10 mm. The rotor and stator materials are carbon steel and silicon steel sheets, respectively. The stator windings occupy 12 stator slots. Table 1 presents the constant values for the AFPMG design.

The primary dimensions of the AFPMG topology were aligned with those of the RFPMG by assigning identical values to certain parameters, including the permanent magnet volume, stator slot width, stator slot height, stator yoke width, stator core length, number of stator turns, wire diameter, and those listed in Table 1. By considering all these parameter limitations, the other dimensions of the AFPMG and RFPMG for each power capacity can then be calculated, with the results shown in Tables 2 and 3, respectively. The same superscript letters in the two tables mean the machine's parts have the same size.

The values of air gap length, slot opening height, and slot wedge height are determined based on manufacturing considerations, and a pole width-to-pole pitch ratio of 0.68 is chosen to minimize the leakage

flux between the permanent magnets [27]. From Tables 2 and 3, we can see that the rise in output power is always followed by an increase in stator core length, which also increases the dimensions of the other active parts of the machine, the rotor, and the permanent magnet.

Figure 1 shows the 3D model of the generator parts for AFPMG in Figure 1(a) and RFPMG in Figure 1(b). The non-overlap fractional slot winding type is selected considering several advantages, as explained in [28]-[30]. The winding is designed based on the double-layer star of slot approach. It is arranged by  $N_s/\delta$  (3 spokes), with  $\delta$  is the greatest common divider (GCD) between the stator slot number  $N_s$  and the number of pole pairs  $p$ . The symbol  $\delta$  also portrays the generator periodicity, which illustrates the number of identical sections of the generator that could be split. The winding data of the observed generators is shown in Table 4.

Table 1. The value of some constant parameters of AFPMG design

No.	Parameters	Value	Unit
1	Air gap length	2	mm
2	Permanent magnet thickness	10	mm
3	Phase numbers	3	phases
4	Phase internal voltage	17	V
5	Phase terminal voltage	15	V
6	Output power	300	W
7	Ampere loading	18,000	A/m
8	Power factor	0.85	
9	Efficiency	0.9	
10	Number of coil per pole per phase	1	coil
11	Ratio of inner to outer diameter	0.577	
12	Slot opening height	2	mm
13	Slot wedge height	2	mm
14	Pole width to pole pitch ratio	0.68	
15	Slot fill factor	0.4	
16	Current density	$4.5 \cdot 10^6$	A/m <sup>2</sup>
17	Maximum flux density of the stator teeth	2	T
18	Maximum flux density of the stator yoke	1.5	T

Table 2. Dimension of the AFPMG according to its capacity

No.	Machine's parts	Generator capacities (W)					Unit
		300	600	900	1200	1500	
1	Outer diameter	160	200	230	250	270	mm
2	Inner diameter	90	120	130	150	160	mm
3	Radial core length (A)	35	40	50	50	55	mm
4	Inner slot width (B)	13	18	20	22	24	mm
5	Outer slot width (C)	13	18	20	22	24	mm
6	Slot height (D)	11	10	14	12.5	14	mm
7	Stator yoke width (E)	14	18	21	23	25	mm
8	Rotor yoke width	14	18	21	23	25	mm
9	Slot opening (F)	3.55	5.08	6.60	7.38	8.13	mm
10	Air gap area	1718.06	2513.27	3534.29	3926.99	4643.67	mm <sup>2</sup>
11	PM volume (G)	11682.80	17090.26	24033.18	26703.54	31576.93	mm <sup>3</sup>

Table 3. Dimension of the RFPMG according to its capacity

No.	Machine's parts	Generator capacities (W)					Unit
		300	600	900	1200	1500	
1	Rotor inner diameter	87	105.78	117.38	133.04	143.26	mm
2	Rotor outer diameter	115	150	170	190	205	mm
3	Stator inner diameter	139	174	194	214	229	mm
4	Stator outer diameter	197	238	268	293	311	mm
5	Axial core length (A)	35	40	50	50	55	mm
6	Inner slot width (B)	13	18	20	22	24	mm
7	Outer slot width (C)	13	18	20	22	24	mm
8	Slot height (D)	11	10	14	12.5	12	mm
9	Stator yoke width (E)	14	18	21	23	25	mm
10	Rotor yoke width	18.05	22.6	26.31	28.48	30.87	mm
11	Slot opening (F)	3.55	5.08	6.60	7.38	8.13	mm
12	Air gap area	1882.99	2701.77	3769.91	4162.61	4902.85	mm <sup>2</sup>
13	PM volume (G)	11682.80	17090.26	24033.18	26703.54	31576.93	mm <sup>3</sup>

Table 4. Winding numbers and conductor sizes for AFPMG and RFPMG

No.	Descriptions	Generator capacities (W)					Unit
		300	600	900	1200	1500	
1	Winding diameter	1.42	2.03	2.64	2.95	3.25	mm
2	Phase winding numbers	72	48	36	32	28	Turns

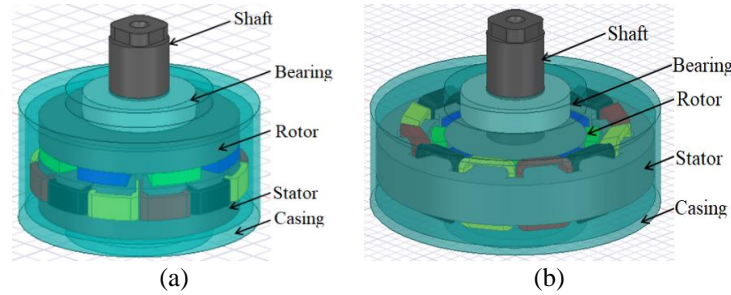


Figure 1. Generators in a 3D model: (a) single-side AFPMG and (b) internal rotor RFPMG

### 2.3. Performance simulation

The finite element analysis (FEA) simulation allows static and dynamic scenarios. Ansys Maxwell uses a specific term for static simulation, namely magnetostatic simulation, referring to a static magnetic field. This study performs both types of simulations.

Figure 2 illustrates the wiring diagram for dynamic simulation, with the machine's characteristics analyzed including the induction voltage  $E_o$ , phase current  $I_a$ , voltage regulation  $V_R$ , total harmonic distortion THD, output power  $P_o$ , efficiency  $\eta$ , electromagnetic torque  $T_e$ , and peak cogging torque  $T_{cog}$ . In this study, all these parameters are obtained with the assistance of Ansys Maxwell software, as detailed in Figure 2. In the simulation, the machine is loaded with a resistive load (RLoad) whose value is adjusted to achieve the desired output power at 835 rpm. The values of RLoad and the corresponding output power for all observed capacities are 2.135  $\Omega$  for 300 W, 1.066  $\Omega$  for 600 W, 0.8531  $\Omega$  for 900 W, 0.6122  $\Omega$  for 1200 W, and 0.5231  $\Omega$  for 1500 W, consecutively.

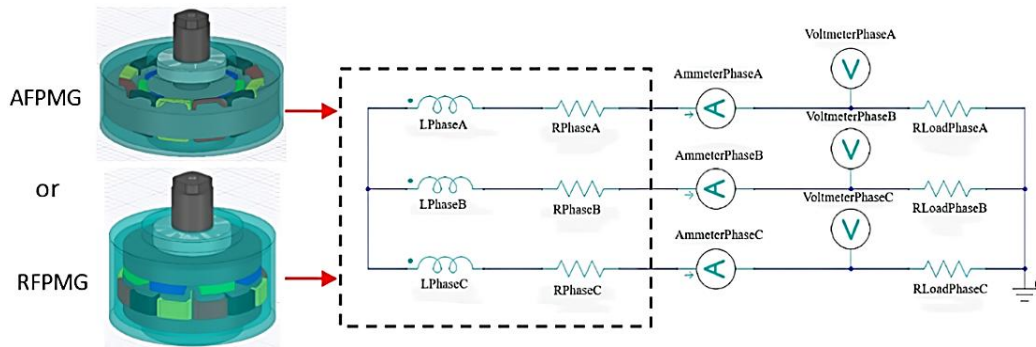


Figure 2. Dynamic simulation by connecting the PMG to the resistive load

### 2.4. Mathematical equations

The following are the mathematical equations used to analyze the machine's performance. The Ansys Maxwell software computes some parameters directly, such as synchronous inductance, air gap flux density, cogging torque, and phase induction voltage. In this regard, the equations presented below are general equations applicable to both AFPMG and RFPMG, containing factors that explain the differences between the observed parameters of the two generator types. Meanwhile, the software generates equations for other parameters, but the designer must input the required factors. The parameters calculated using these equations include armature current, terminal voltage, output power, and electromagnetic torque.

The synchronous inductance  $L_s$ , that equals to  $L_{\text{phase A/B/C}}$  in Figure 2, is given by (1) and (2) [31], [32].

$$L_s = L_k + L_m \quad (1)$$

$$L_m = \frac{\psi_{m(i)}}{I_m} = \frac{\psi_{m(i)}}{H_c h_m} \quad (2)$$

Subsequently, (3)-(5) elucidate the process of obtaining the phase induction voltage  $E_f$ , which involves first calculating the magnetic flux  $\phi_f$  and flux linkage  $\psi_m$  [11], [33].

$$\phi_f = B_g A_g \quad (3)$$

$$\psi_m = k_w N_1 \phi_f \quad (4)$$

$$E_f = \pi \sqrt{2} f \psi_m \quad (5)$$

Cogging torque  $T_{cog}$  is expressed by [34] and air gap reluctance  $\mathcal{R}$  is obtained from the equation in Ansys Maxwell software.

$$T_{cog} = -\frac{1}{2} \phi_m^2 \frac{d\mathcal{R}}{d\theta} \quad (6)$$

$$\mathcal{R} = \frac{\oint_{gap} H \cdot dl}{\int_{gap} B \cdot n \cdot dA} \quad (7)$$

The next parameters are the armature current  $I_a$ , terminal voltage  $V_T$ , winding loss  $P_R$ , output power  $P_o$ , electromagnetic torque  $T_e$  and electromagnetic power  $P_e$ , [35], [36].

$$I_a = \frac{E_f}{\sqrt{(R_a + R_{Load})^2 + (X_s)^2}} \quad (8)$$

$$V_T = I_a R_{Load} \quad (9)$$

$$P_R = 3 I_a^2 R_a \quad (10)$$

$$P_o = m V_T I_a \cos \beta \quad (11)$$

$$T_e = \frac{P_e}{2\pi n_s} \quad (12)$$

$$P_e = P_o + P_R + P_c \quad (13)$$

Where  $L_k$  is the leakage inductance,  $L_m$  is the magnetic inductance,  $I_m$  is the field excitation current,  $\psi_{m(i)}$  is the flux linkage at current  $i$ ,  $H_c$  is the coercive force,  $h_m$  is the magnet thickness,  $A_g$  is the air gap area,  $k_w$  is the winding factor,  $N_1$  is the phase winding numbers,  $\theta$  is the rotor position angle,  $H$  is the magnetic field strength of permanent magnet,  $l$  is the length of the magnetic flux path,  $B \cdot n$  denotes the normal component of  $B$  to the surface element  $dA$  and is thus considered in the calculation,  $X_s$  is the synchronous reactance,  $R_a$  is the armature resistance = RPhasaA/B/C in Figure 2, Rload is the resistive load,  $m$  is the phase number,  $\cos \beta$  is the power factor angle = 1,  $n_s$  is the rotor speed in rev/s,  $P_c$  is the coreloss.

### 3. RESULTS AND DISCUSSION

This section analyzes the winding and the no-load magnetic characteristics first, followed by the electrical and mechanical performances. Detailed parameters investigated are described in each section.

#### 3.1. Winding parameters

The simulation results of winding parameters based on the capacity of each topology are shown in Table 5. It can be seen from Table 5 that at the same capacity, the armature resistance  $R_a$  of RFPMG has a higher value than AFPMG since its phase winding is longer, causing greater winding weight. The succeeding parameter is synchronous inductance  $L_s$ , exhibiting  $L_s$  values of RFPMG are higher across all power capacities. One of the factors influencing  $L_s$  is  $L_k$  as in (1), whose value is affected by the stator dimensions, especially slot shape and size. Hence, we may assume that the  $L_k$  of both topologies is the same. Meanwhile,  $I_m$ , in (2), is the same for both topologies because of the same  $H_c$  and  $h_m$ . Therefore,  $L_m$  or  $L_s$  is only affected by  $\psi_{m(i)}$ , which is consistently higher in RFPMG at all power levels as discussed in section 3.3.

Table 5. Winding parameters according to its capacity

No.	Descriptions		Generator capacities (W)					Unit
			300	600	900	1200	1500	
1	Armature resistance, $R_a$	AFPMG	0.320	0.132	0.069	0.052	0.041	$\Omega$
		RFPMG	0.406	0.155	0.080	0.060	0.046	$\Omega$
2	Synchronous inductance, $L_s$	AFPMG	436.60	207.50	132.75	108.02	90.55	$\mu\text{H}$
		RFPMG	437.36	219.79	147.45	116.36	94.12	$\mu\text{H}$
3	The length of winding per phase	AFPMG	8.96	7.56	6.69	6.24	5.94	m
		RFPMG	11.31	8.83	7.72	7.15	6.63	m
4	Weight of the winding	AFPMG	$2.57 \cdot 10^4$	$3.11 \cdot 10^4$	$3.80 \cdot 10^4$	$4.41 \cdot 10^4$	$5.28 \cdot 10^4$	$\text{mm}^3$
		RFPMG	$3.08 \cdot 10^4$	$3.50 \cdot 10^4$	$4.21 \cdot 10^4$	$4.88 \cdot 10^4$	$5.73 \cdot 10^4$	$\text{mm}^3$

### 3.2. No-load characteristics

Table 6 displays three parameters, namely average air gap flux density  $B_{gave}$ , average magnetic flux  $\phi_{mave}$ , and  $\psi_m$ . The  $B_{gave}$  values are obtained from the Ansys Maxwell magnetostatic simulation, and then by using (3) and (4),  $\phi_{mave}$  and  $\psi_m$  are calculated. It can be seen in Table 6 that the  $B_{gave}$  at no load for AFPMG is higher than that of the RFPMG.

The following factors are  $\phi_{mave}$  and  $\psi_m$ , indicating similar or slightly lower values in the AFPMG topology than the RFPMG. Although the AFPMG has a higher  $B_{gave}$  than the RFPMG, its little air gap area  $A_g$  (see Tables 2 and 3, respectively) results in smaller  $\phi_{mave}$  and  $\psi_m$  compared to RFPMG as in (3) and (4). Figure 3 shows a comparison of the no-load characteristics of  $E_o$  in Figure 3(a) and  $T_{cog}$  in Figure 3(b). In Figure 3(a), we can see that the smaller values of  $\phi_{mave}$  and  $\psi_m$  from AFPMG affect the  $E_o$ , which exhibits a greater value for RFPMG than AFPMG. The nonlinearity of the  $E_o$  graph to power variation results from the influence of  $N_1$  as in (4), whose value is strategically tuned to reach an approximation  $E_o$  of 17 V.

The percentage differences presented are absolute values. The graph in Figure 3 shows that the difference in  $E_o$  values between the two generator types is relatively stable with increasing power, with an average value of 3.47%. These results contrast with those obtained in [24] because the AFPMG used in the study was a double-sided coreless type, compared to a conventional RFPMG.

Table 6. No load  $B_{gave}$ ,  $\phi_{mave}$ , and  $\psi_m$ 

No.	Descriptions		Generator capacities (W)					Unit
			300	600	900	1200	1500	
1	$B_{gave}$	AFPMG	0.648	0.653	0.642	0.632	0.631	T
		RFPMG	0.604	0.611	0.616	0.618	0.612	T
2	$\phi_{mave}$	AFPMG	0.0011	0.0016	0.0023	0.0025	0.0029	Wb
		RFPMG	0.0011	0.0017	0.0023	0.0026	0.0030	Wb
3	$\psi_m$	AFPMG	0.0686	0.0665	0.0717	0.0693	0.0703	Wb
		RFPMG	0.0686	0.0707	0.0717	0.0721	0.0727	Wb

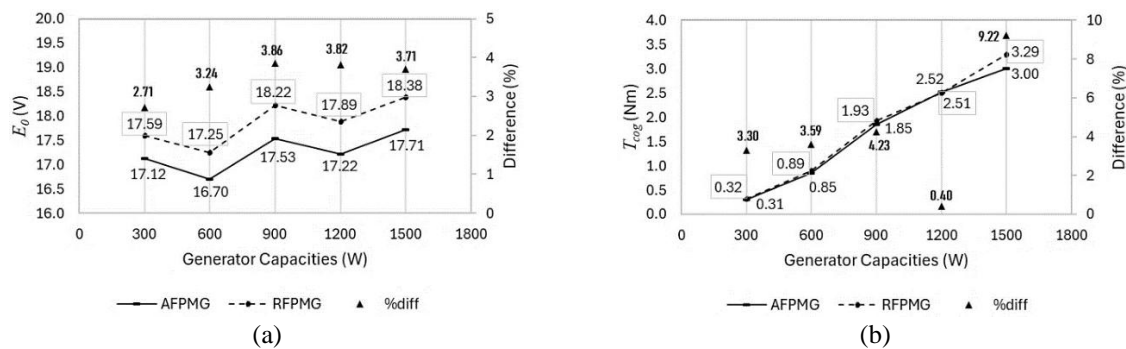
Figure 3. Comparison of no-load characteristics of (a)  $E_o$  and (b)  $T_{cog}$ 

Figure 3(b) shows that the  $T_{cog}$  curves of AFPMG and RFPMG generally overlap across all power levels, with RFPMG exhibiting higher values except at 1200 W. According to (6) and (7), this trend is influenced by two factors: magnetic flux ( $\phi_m$ ) and reluctance variation ( $d\mathcal{R}/d\theta$ ). As shown in Table 6,  $\phi_m$  does not align with the  $T_{cog}$  pattern, highlighting the importance of  $d\mathcal{R}/d\theta$ . In (7), reluctance  $\mathcal{R}$  depends on flux density  $B$  and magnetic path length  $l$ , while  $H$  remains constant for both machines due to identical magnet strength. The AFPMG likely has a shorter  $l$ , as suggested by its reduced stator winding length (Table 5). The relationship between  $d\mathcal{R}/d\theta$  and  $B$  is reflected in the crest shape of the air-gap flux density

waveform (supplementary document). At 300–900 W and 1500 W, AFPMG exhibits smoother waveforms, indicating lower  $d\mathcal{R}/d\theta$  and consequently lower  $T_{cog}$ , whereas RFPMG shows slight ripples. However, at 1200 W, AFPMG displays higher  $d\mathcal{R}/d\theta$ , resulting in a higher  $T_{cog}$  than RFPMG. The average cogging torque difference between the two machines from 300–1200 W is 2.88%, while at 1500 rpm, RFPMG's  $T_{cog}$  increases sharply due to higher  $\phi_m$  and  $d\mathcal{R}/d\theta$ , reaching the most significant difference of 9.22%. Overall, RFPMG, with its radial air gap, generates a less uniform flux distribution compared to the planar air gap of AFPMG, and the torque discrepancy tends to grow with increasing power, with RFPMG prone to exhibit higher values.

### 3.3. On-load characteristics

Table 7 presents the on-load simulation results of  $\psi_{m(i)}$ ,  $E_{f(i)}$ ,  $I_a$  and  $P_R$  with the loading method described in section 2.2. using the loading method described in section 2.2. The software computes the parameters of  $\psi_{m(i)}$  and  $E_{f(i)}$  through dynamic simulation. The  $E_{f(i)}$  values displayed in the table are in rms. Next, (8) and (10) are applied to calculate  $I_a$  and  $P_R$ , respectively.

From Table 7, we can observe that  $\psi_{m(i)}$  is proportional to  $E_{f(i)}$ , and the  $E_{f(i)}$  of the RFPMG is consistently higher than that of the AFPMG. Meanwhile,  $I_a$  is influenced by three dividing factors, namely  $R_a$ ,  $R_{Load}$ , and  $L_s$ . The calculations show that at 300 W, the result differs, with the  $I_a$  of the RFPMG being lower than that of the AFPMG, while at other capacities, it is higher. These findings indicate that the impact of  $R_s$  and  $X_s$  on  $I_a$  in the RFPMG is more prominent at lower power levels for winding loss, the RFPMG yields higher values than the AFPMG at all capacities, which is proportional to its  $R_a$ , even though its  $I_a$  is slightly lower at 300 W.

The following is Figure 4, which exhibits the terminal voltage  $V_T$  at each observed power level.  $V_T$  is calculated using (9), and the results show that the RFPMG has a higher  $V_T$  at all capacities except at 300 W. This is consistent with the current  $I_a$  pattern, as  $V_T$  is proportional to  $I_a$ . As explained above,  $R_s$  and  $X_s$  strongly affect  $I_a$  in the RFPMG at low power levels. However, their influence progressively weakens with increasing power, as  $E_{f(i)}$  consistently remains higher, allowing the RFPMG to achieve a higher terminal voltage than the AFPMG under high-power scenarios.

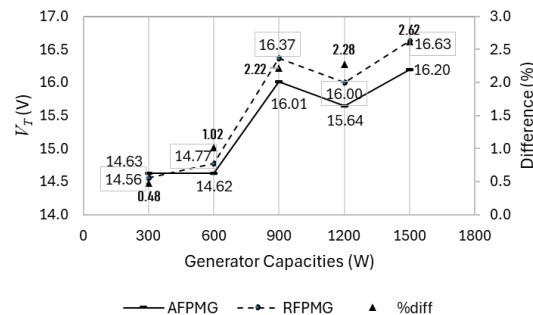


Figure 4. Terminal voltage

The trend in the graph shown in Figure 4 indicates that at power levels above 300 W up to 1500 W, the  $V_T$  of the RFPMG is consistently higher than that of the AFPMG (in agreement with the findings of [22]), with the percentage difference tending to increase, reaching a maximum difference of 2.62% at 1500 W. However, at power levels below 300 W, the  $V_T$  of the RFPMG is lower than that of the AFPMG, and this will likely continue to be the case.

From the value of  $E_o$  and  $V_T$ , we can determine the voltage regulation, which represents the voltage change from no-load to on-load conditions. Table 8 presents the simulation results for VR and THD. VR is expressed as a percentage, where a lower VR indicates a smaller voltage drop and better voltage quality. The simulation results for VR in Table 8 show that the VR of the AFPMG is better than that of the RFPMG. The percentage difference in VR decreases as the power increases, with maximum and minimum values of 20.04% and 12.12%, corresponding to 300 W and 1500 W, respectively. This trend suggests the possibility that at higher power levels, the VR of the RFPMG may match or even be lower than that of the AFPMG.

The next factor is THD, which reflects the voltage waveform quality or how closely the waveform approaches a sinusoidal shape. Table 8 shows that the AFPMG exhibits lower THD than the RFPMG because its trapezoidal coil produces a more sinusoidal voltage waveform than the square-shaped coil of the RFPMG. The minimum and maximum percentage differences in THD occur at 1200 W and 1500 W, with 11.24% and 13.93%, respectively. There is no specific pattern in the THD values concerning power changes; the values fluctuate randomly, but the THD of the AFPMG consistently remains lower.

Table 9 lists the core volume and core loss, which are proportional to the output power. The rate of change in core volume increases as output power increases. The percentage differences in core volume and  $P_c$  with increasing capacity do not follow a specific feature. However, in both cases, the AFPMG performs better than the RFPMG. The average percentage differences are 29.77% for core volume and 1.45% for  $P_c$ . These results are consistent with those obtained in [21] and [24].

Table 7. The values of  $\psi_{m(i)}$ ,  $E_{fi(i)}$ ,  $I_a$ , and  $P_R$ 

No.	Descriptions		Generator capacities (W)					Unit
			300	600	900	1200	1500	
1	$\psi_{m(i)}$	AFPMG	0.0696	0.0680	0.0717	0.0704	0.0724	Wb
		RFPMG	0.0718	0.0702	0.0744	0.0730	0.0751	Wb
2	$E_{fi(i)}$	AFPMG	16.83	16.44	17.31	16.99	17.48	V
		RFPMG	17.33	16.93	17.91	17.57	18.08	V
3	$I_a$	AFPMG	6.85	13.72	18.77	25.55	30.98	A
		RFPMG	6.82	13.86	19.19	26.14	31.78	A
4	$P_R$	AFPMG	45.12	74.32	72.85	102.55	117.63	W
		RFPMG	56.54	89.12	88.52	122.79	137.94	W

Table 8.  $V_R$  and THD

No.	Descriptions		Generator capacities (W)					Unit
			300	600	900	1200	1500	
1	VR	AFPMG	17.02	14.23	9.49	10.10	9.32	%
		RFPMG	20.81	16.79	11.30	11.81	10.52	%
2	THD	AFPMG	9.49	10.55	10.98	11.17	11.02	%
		RFPMG	10.86	11.91	12.51	12.5	12.67	%

Table 9. Core volume and coreloss

No.	Descriptions		Generator capacities (W)					Unit
			300	600	900	1200	1500	
1	Core volume	AFPMG	0.00033	0.00054	0.00091	0.00105	0.00130	m <sup>3</sup>
		RFPMG	0.00047	0.00073	0.00124	0.00138	0.00169	m <sup>3</sup>
2	Coreloss, $P_c$	AFPMG	7.38	11.88	17.57	23.14	26.34	W
		RFPMG	7.39	12.72	19.25	25.24	29.43	W

Figure 5 displays the load characteristics of  $P_o$  and  $T_e$  in Figures 5(a) and 5(b), respectively. Figure 5(a) shows that at low power (300 W), the  $P_o$  of the RFPMG is lower than that of the AFPMG, but beyond that point, it is consistently higher, with an average difference of around 3.42%. Despite having higher  $P_R$  and  $P_c$  than the AFPMG, the  $P_o$  of the RFPMG, particularly in the 600 W–1500 W range, is higher due to its higher  $I_a$  and  $V_T$  as in (11). The results obtained in this power range are consistent with those in [26], but that study applied a mechanical energy storage system. The trend in the graph in Figure 5 also indicates that at higher power levels, the percentage difference in  $P_o$  between the RFPMG and AFPMG may continue to increase. Meanwhile, at power levels up to 300 W, the AFPMG may produce a higher  $P_o$ . Thus,  $I_a$ ,  $V_T$ , and  $P_o$  exhibit similar trends in value changes in response to power variations.

The electromagnetic torque  $T_e$  shown in Figure 5(b) represents the torque in the air gap. From (12) and (13), it can be seen that  $T_e$  is proportional to the sum of  $P_o$ ,  $P_R$ , and  $P_c$ , which causes the RFPMG to produce higher  $T_e$  than the AFPMG across all capacities. Even at 300 W, where the  $I_a$  of the RFPMG is slightly lower, the  $T_e$  generated is still higher. The percentage difference in  $T_e$  with varying power levels is irregular, fluctuating randomly without a clear pattern. A slighter  $T_e$  requires a lower prime mover capacity, making the power generation system more cost-effective.

Figure 6 shows a comparison of efficiency in Figure 6(a) and power density in Figure 6(b). In Figure 6(a), we can see that the AFPMG displays higher efficiency than the RFPMG. The graph also indicates an inverse correlation between increasing power and the percentage difference. In other words, the higher the power, the smaller the percentage difference. It enables the RFPMG's efficiency to match or surpass the AFPMG at a higher power level. These results are consistent with those reported in [21]. On the other hand, a study by [25] found equal efficiency between the AFPMG and RFPMG, but the RFPMG used a spoke permanent magnet inner rotor design.

The final parameter is the power density  $P_D$ , as shown in Figure 6(b). Due to its minor core volume (although with lower  $P_o$ ), the  $P_D$  of the AFPMG is better than that of the RFPMG, consistent with the findings in [21]. From the figure, we can observe a tendency for the percentage difference in  $P_D$  to decrease, but overall, both curves remain parallel.

Beyond performance metrics like power density, practical factors such as ease of manufacturing are crucial for real-world applications. AFPMG typically offers a more inelaborate, compact stator-rotor design and easier assembly, but it requires precise axial flux alignment for uniform air gap distribution. In contrast, RFPMG follows a conventional radial design, benefiting from mass production efficiency but requiring more complex winding arrangements.

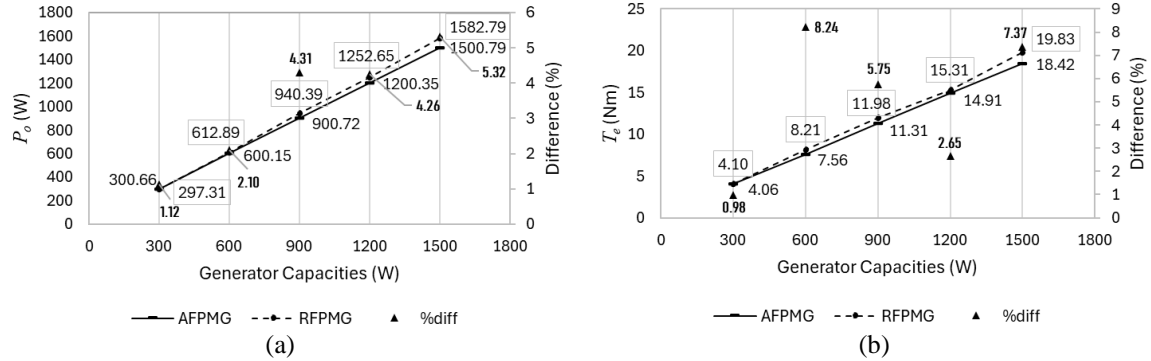


Figure 5. On-load characteristics of (a) output power and (b) electromagnetic torque

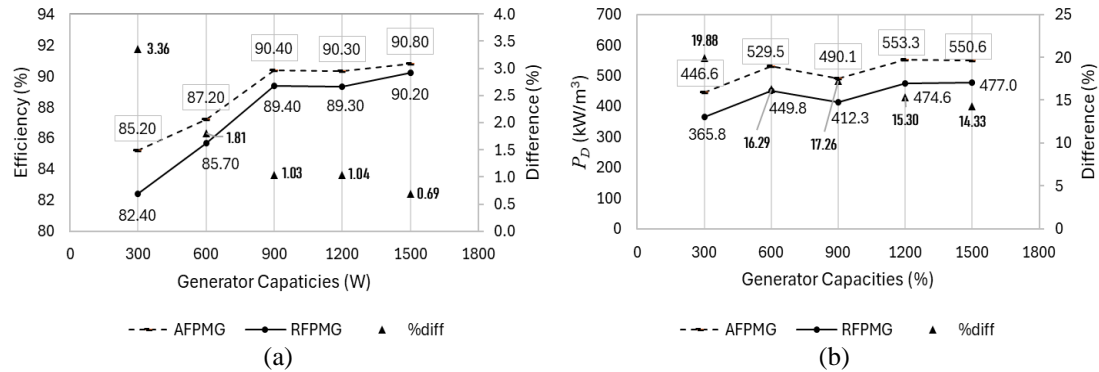


Figure 6. The comparison of (a) efficiency and (b) power density

#### 4. CONCLUSION

This paper compares the performance of AFPMG and RFPMG across five different power capacities. The generator topologies are single-gap AFPMG and single-gap inner rotor RFPMG. The study aims to identify how the primary parameters vary at each power capacity and observe the trends in their values as power changes. The simulations used Ansys Maxwell software to obtain the no-load and on-load characteristics.

The analysis reveals that AFPMG performs better for most analyzed parameters, including cogging torque, voltage regulation, THD, electromagnetic torque, efficiency, and power density. Meanwhile, RFPMG exhibits superior performance in terminal voltage and output power. Notably, for the RFPMG, the percentage difference in output power compared to the AFPMG tends to increase at high power levels, with efficiency improving closer to that of the AFPMG. However, this improvement also results in higher electromagnetic torque and cogging torque.

These findings conclude that the AFPMG outperforms the RFPMG at each observed power capacity, both technical performance and economic feasibility. It is also more suitable for wind or hydropower applications. While this study provides an in-depth comparative analysis using finite element simulations, experimental validation is still required to confirm real-world applicability. Additionally, a more detailed cost-benefit analysis would further enhance the economic feasibility assessment of both generator topologies. However, prototype fabrication across multiple power capacities involves significant complexity and resource requirements, while extensive cost evaluation requires detailed data on material costs, production processes, and a detailed industry assessment. Therefore, experimental validation and economic analysis will be considered in future work to support the findings presented here.

## FUNDING INFORMATION

Authors state no funding involved.

## AUTHOR CONTRIBUTIONS STATEMENT

This journal uses the Contributor Roles Taxonomy (CRediT) to recognize individual author contributions, reduce authorship disputes, and facilitate collaboration.

Name of Author	C	M	So	Va	Fo	I	R	D	O	E	Vi	Su	P	Fu
Ketut Wirtayasa	✓		✓			✓		✓	✓		✓			
Muhammad Kasim	✓			✓	✓		✓			✓				
Puji Widiyanto			✓			✓	✓	✓	✓		✓			
Anwar Muqorobin		✓		✓		✓				✓				
Sulistyo Wijanarko					✓					✓				
Pudji Irasari	✓	✓		✓	✓				✓		✓			

C : Conceptualization

M : Methodology

So : Software

Va : Validation

Fo : Formal analysis

I : Investigation

R : Resources

D : Data Curation

O : Writing - Original Draft

E : Writing - Review & Editing

Vi : Visualization

Su : Supervision

P : Project administration

Fu : Funding acquisition

## CONFLICT OF INTEREST STATEMENT

Authors state no conflict of interest.

## DATA AVAILABILITY

The authors confirm that the data supporting the findings of this study are available within the article [and/or its supplementary materials].




## REFERENCES

- [1] K. Salihi, M. Q. Taha, A. Oubeidi, M. Ndongo, S. Ben Jabrallah, and B. El Heiba, "Planning optimization of a standalone photovoltaic/diesel/battery energy system for a gold mining location in Mauritania," *Engineering, Technology & Applied Science Research*, vol. 14, no. 4, pp. 15637–15644, Aug. 2024, doi: 10.48084/etasr.7776.
- [2] M. Q. Taha, I. C. Elhassene, and B. El Heiba, "Gray wolf algorithm optimization of automatic generation control for deregulated multi-area power system," *HORA 2024 - 6th International Congress on Human-Computer Interaction, Optimization and Robotic Applications, Proceedings*, pp. 1–4, 2024, doi: 10.1109/HORA61326.2024.10550602.
- [3] M. Q. Taha, B. El Heiba, and I. C. Elhassene, "Performance assessment of multiple optimizing algorithms for hybrid PV and diesel energy system sizing," *International Journal of Energy Production and Management*, vol. 9, no. 3, Sep. 2024, doi: 10.18280/ijepm.090303.
- [4] H. J. Park, H. L. Kang, D. G. Ahn, and S. H. Han, "Optimal shape design of direct-drive permanent magnet generator for 1 kW-class wind turbines," *Applied Sciences*, vol. 13, no. 10, p. 5856, May 2023, doi: 10.3390/app13105856.
- [5] G. Ahmad and U. Amin, "Design, construction and study of small scale vertical axis wind turbine based on a magnetically levitated axial flux permanent magnet generator," *Renewable Energy*, vol. 101, Feb. 2017, doi: 10.1016/j.renene.2016.08.027.
- [6] S. J. Arand and M. Ardebili, "Cogging torque reduction in axial-flux permanent magnet wind generators with yokeless and segmented armature by radially segmented and peripherally shifted magnet pieces," *Renewable Energy*, vol. 99, pp. 95–106, Dec. 2016, doi: 10.1016/j.renene.2016.06.054.
- [7] K. Wirtayasa and C.-Y. Hsiao, "Performances comparison of axial-flux permanent-magnet generators for small-scale vertical-axis wind turbine," *Alexandria Engineering Journal*, vol. 61, no. 2, pp. 1201–1215, Feb. 2022, doi: 10.1016/j.aej.2021.06.074.
- [8] M. Chirca, C. Oprea, P.-D. Teodosescu, and S. Breban, "Optimal design of a radial flux spoke-type interior rotor permanent magnet generator for micro-wind turbine applications," in *2016 International Conference on Applied and Theoretical Electricity (ICATE)*, IEEE, Oct. 2016, pp. 1–5, doi: 10.1109/ICATE.2016.7754645.
- [9] V. Di Dio, G. Cipriani, and D. Manno, "Axial flux permanent magnet synchronous generators for Pico hydropower application: a parametrical study," *Energies*, vol. 15, no. 19, p. 6893, Sep. 2022, doi: 10.3390/en15196893.
- [10] V. P. Chandran, S. Murshid, and B. Singh, "Improved TOGI-based voltage and frequency control for PMSG feeding single-phase loads in isolated Pico-hydro generation," *IETE Journal of Research*, vol. 67, no. 6, Nov. 2021, doi: 10.1080/03772063.2019.1571953.
- [11] P. Irasari, A. Muqorobin, P. Widiyanto, T. Nur, I. N. Diasta, and P. Soetikno, "Performance analyzes of a compact pico hydropower plant with a wide operating range," *International Journal of Power Electronics and Drive Systems (IJPEDS)*, vol. 13, no. 4, pp. 2357–2364, Dec. 2022, doi: 10.11591/ijpeds.v13.i4.pp2357-2364.
- [12] E. Flores, M. Cumbajin, and P. Sanchez, "Design of a synchronous generator of permanent magnets of radial flux for a Pico-hydropower station," in *Advances and Applications in Computer Science, Electronics and Industrial Engineering*, 2021, pp. 135–151, doi: 10.1007/978-981-33-4565-2\_9.
- [13] Y. Dai, D.-W. Lee, H.-K. Joung, and H.-J. Lee, "Optimization on torque ripple performance in ISG motors with fractional slot distributed windings and rotor notching," *IEEE Access*, vol. 12, pp. 123872–123882, 2024, doi: 10.1109/ACCESS.2024.3433452.
- [14] Z. Islam, F. Khan, B. Ullah, A. H. Milyani, and A. A. Azhari, "Design and analysis of three phase axial flux permanent magnet machine with different PM shapes for electric vehicles," *Energies*, vol. 15, no. 20, p. 7533, Oct. 2022, doi: 10.3390/en15207533.




- [15] M. Kasim and J. Fletcher, "Mechanical field weakening techniques for an axial flux machine," in *2019 International Conference on Sustainable Energy Engineering and Application (ICSEEA)*, IEEE, Oct. 2019, pp. 7–15. doi: 10.1109/ICSEEA47812.2019.8938626.
- [16] M. Bharathi, U. B. Akuru, and M. K. Kumar, "Comparative design and performance analysis of 10 kW rare-earth and non-rare earth flux reversal wind generators," *Energies*, vol. 15, no. 2, p. 636, Jan. 2022, doi: 10.3390/en15020636.
- [17] T.-K. Hoang, L. Vido, and C. Tchuanglong, "Torque ripple and mass comparison between 20 MW rare-earth and ferrite permanent magnet wind generators," *Machines*, vol. 11, no. 12, p. 1063, Nov. 2023, doi: 10.3390/machines11121063.
- [18] S. Amin, S. Madanzadeh, S. Khan, S. S. H. Bukhari, F. Akhtar, and J.-S. Ro, "Effect of the magnet shape on the performance of coreless axial flux permanent magnet synchronous generator," *Electrical Engineering*, vol. 104, no. 2, pp. 959–968, Apr. 2022, doi: 10.1007/s00202-021-01338-x.
- [19] D. Slutskiy, S. H. Aung, and S. Basnet, "Comparison of axial and radial flux permanent magnet machines," *2022 North American Power Symposium, NAPS 2022*, pp. 1–6, 2022, doi: 10.1109/NAPS56150.2022.10012265.
- [20] R. Tsunata, M. Takemoto, J. Imai, T. Saito, and T. Ueno, "Comparison of thermal characteristics in various aspect ratios for radial-flux and axial-flux permanent magnet machines," *IEEE Transactions on Industry Applications*, vol. 59, no. 3, pp. 3353–3367, May 2023, doi: 10.1109/TIA.2023.3255845.
- [21] O. Bouaziz, I. Jaafar, and F. Ben Ammar, "Performance analysis of radial and axial flux PMSM based on 3D FEM modeling," *Turkish Journal of Electrical Engineering and Computer Sciences*, vol. 26, no. 3, pp. 1587–1598, May 2018, doi: 10.3906/elk-1708-68.
- [22] V. de A. Neumann and R. P. Homrich, "Comparison between radial and axial permanent magnet generators for low speed application," in *2014 IEEE International Instrumentation and Measurement Technology Conference (I2MTC) Proceedings*, IEEE, May 2014, pp. 251–256. doi: 10.1109/I2MTC.2014.6860746.
- [23] M. R. Dubois, H. Polinder, and J. A. Ferreira, "Axial and radial-flux permanent magnet generators for direct-drive wind turbines," in *Proceedings of the European Wind Energy Conference 2001*, pp. 1112–1115, 2001.
- [24] B. Sitheswaran, S. Pandarinathan, M. Alagu, and P. Ponnusamy, "Performance analysis of radial flux and axial flux permanent magnet generators for low-speed wind turbine applications," *International Journal of Applied Electromagnetics and Mechanics*, vol. 65, no. 1, pp. 129–147, Jan. 2021, doi: 10.3233/JAE-190150.
- [25] A. A. Pop, F. Jurca, C. Oprea, M. Chirca, S. Breban, and M. M. Radulescu, "Axial-flux vs. radial-flux permanent-magnet synchronous generators for micro-wind turbine application," in *2013 15th European Conference on Power Electronics and Applications (EPE)*, IEEE, Sep. 2013, pp. 1–10. doi: 10.1109/EPE.2013.6634639.
- [26] Y.-S. Park, M.-M. Koo, S.-M. Jang, J.-Y. Choi, and D.-J. You, "Performance evaluation of radial- and axial-flux PM wind power generators with mechanical energy storage system," *IEEE Transactions on Energy Conversion*, vol. 30, no. 1, pp. 237–245, Mar. 2015, doi: 10.1109/TEC.2014.2331246.
- [27] T. Asefi, J. Faiz, and M. A. Khan, "Design of dual rotor axial flux permanent magnet generators with ferrite and rare-earth magnets," in *2018 IEEE 18th International Power Electronics and Motion Control Conference (PEMC)*, IEEE, Aug. 2018, pp. 531–538. doi: 10.1109/EPEPEMC.2018.8522004.
- [28] X. Chen and J. Wang, "Magnetomotive force harmonic reduction techniques for fractional-slot non-overlapping winding configurations in permanent-magnet synchronous machines," *Chinese Journal of Electrical Engineering*, vol. 3, no. 2, pp. 102–113, Sep. 2017, doi: 10.23919/CJEE.2017.8048416.
- [29] A. M. EL-Refaie, M. R. Shah, J. P. Alexander, S. Galioto, K.-K. Huh, and W. D. Gerstler, "Rotor end losses in multiphase fractional-slot concentrated-winding permanent magnet synchronous machines," *IEEE Transactions on Industry Applications*, vol. 47, no. 5, pp. 2066–2074, Sep. 2011, doi: 10.1109/TIA.2011.2162049.
- [30] S. Cai, Z.-Q. Zhu, C. Wang, J.-C. Mipo, and S. Personnaz, "A novel fractional slot non-overlapping winding hybrid excited machine with consequent-pole PM rotor," *IEEE Transactions on Energy Conversion*, vol. 35, no. 3, Sep. 2020, doi: 10.1109/TEC.2020.2978978.
- [31] C. Madariaga, W. Jara, J. A. Tapia, J. Pyrhonen, P. Lindh, and J. A. Riedemann, "Closed-form solution for the slot leakage inductance of tooth-coil-winding permanent magnet machines," *IEEE Transactions on Energy Conversion*, vol. 34, no. 3, pp. 1572–1580, Sep. 2019, doi: 10.1109/TEC.2019.2908053.
- [32] M. Ibrahim and P. Pillay, "The loss of self-excitation capability in stand-alone synchronous reluctance generators," *IEEE Transactions on Industry Applications*, vol. 54, no. 6, pp. 6290–6298, Nov. 2018, doi: 10.1109/TIA.2018.2849407.
- [33] P. Irasari, P. Sutikno, P. Widiyanto, and Q. Maulana, "Performance measurement of a compact generator - hydro turbine system," *International Journal of Electrical and Computer Engineering (IJECE)*, vol. 5, no. 6, pp. 1252–1261, Dec. 2015, doi: 10.11591/ijece.v5i6.pp1252-1261.
- [34] E. Kurt, H. Gör, and K. Çelik, "Optimization of a 3- kW axial flux permanent magnet generator with variable air gap," *International Transactions on Electrical Energy Systems*, vol. 31, no. 11, p. e13074, Nov. 2021, doi: 10.1002/2050-7038.13074.
- [35] J. F. Gieras, R.-J. Wang, and M. J. Kamper, "Principles of AFPM machines," *Axial Flux Permanent Magnet Brushless Machines*, pp. 29–78, 2008, doi: 10.1007/978-1-4020-8227-6\_2.
- [36] K.-H. Shin, T.-K. Bang, H.-W. Cho, and J.-Y. Choi, "Design and analysis of high-speed permanent magnet synchronous generator with rotor structure considering electromechanical characteristics," *IEEE Transactions on Applied Superconductivity*, vol. 30, no. 4, pp. 1–5, Jun. 2020, doi: 10.1109/TASC.2020.2980536.

## BIOGRAPHIES OF AUTHORS






**Ketut Wirtayasa**    is a researcher at the Research Center for Energy Conversion and Conservation, National Research and Innovation Agency, Indonesia. He received his bachelor's degree in electrical engineering from Udayana University in 2007 and his master's degree in energy management from Udayana University in 2012. He finished his Ph.D. in Electrical Engineering at National Taiwan University of Science and Technology (NTUST) in 2022. His research interests include electrical machines and energy management systems. He can be contacted at email: ketu003@brin.go.id.






**Muhammad Kasim**    is a researcher at Research Center for Energy Conversion and Conservation, National Research and Innovation Agency, Indonesia. He received his bachelor's degree in electrical engineering from Hasanuddin University in 2003 and his master's degree in renewable energy from Murdoch University in 2014. He finished his Ph.D. in Electrical Engineering at the School of Electrical Engineering and Telecommunication University of New South Wales in 2022. His research interests include electrical machines and renewable energy management systems. He can be contacted at email: muha087@brin.go.id.






**Puji Widiyanto**    received his B.Eng. and M.Eng. degrees both in Mechanical Engineering, first in STT Mandala and later in Bandung Institute of Technology, Indonesia. Having focused his research on the structure, mechanical design, and manufacture of electrical machines, he is now working as a researcher at the Research Center for Energy Conversion and Conservation, the National Research and Innovation Agency (BRIN). Currently, he is conducting a project on low-head hydropower system. He can be contacted at email: puji010@brin.go.id or pujiwidiyanto@gmail.com.






**Anwar Muqorobin**    studied electrical engineering at Diponegoro University and Bandung Institute of Technology. At present, he is a researcher at the National Research and Innovation Agency (BRIN). His research activities are focused on DC-DC converter, inverter, and control applications. He can be contacted at email: anwa014@brin.go.id.



**Sulistyo Wijnarko**    received his bachelor's degree in Electrical Engineering from Gadjah Mada University in 2013 and his master's degree from the Bandung Institute of Technology in 2021. At present, he is a research assistant at the National Research and Innovation Agency, Indonesia. His field of research is power electronics and drives. He can be contacted at email: sulistyo.wijnarko@brin.go.id.



**Pudji Irasari**    is a researcher at the Research Center for Energy Conversion and Conservation, National Research and Innovation Agency, Indonesia. She received her bachelor's degree in electrical engineering from Brawijaya University in 1994 and her master's degree in renewable energy from Oldenburg University in 2003. Her research interests include electrical machines (motors and generators) and renewable energy-based power generation, particularly wind, water, and ocean energy. She can be contacted at email: pudj003@brin.go.id.